Journal of Solid State Chemistry 345 (2025) 125226

Contents lists available at ScienceDirect

Journal of Solid State Chemistry

journal homepage: www.elsevier.com/locate/yjssc

Deciphering the commensurately modulated monoclinic phase of Rb_2ZnCl_4 at low temperatures

Surya Rohith Kotla [a,*], Sitaram Ramakrishnan [b,1], Achim M. Schaller [a], Toms Rekis [d], Claudio Eisele [a], Jin-Ke Bao [c], Leila Noohinejad [e], Geoffroy de Laitre [f], Marc de Boissieu [f], Sander van Smaalen [a,*]

[a] Laboratory of Crystallography, University of Bayreuth, Universitaetstrasse 30, Bayreuth, 95447, Germany
[b] I-HUB Quantum Technology Foundation, Indian Institute of Science Education and Research, Pune, 411008, India
[c] School of Physics, Hangzhou Normal Univeristy, Hangzhou, 311121, People's Republic of China
[d] Institute of Inorganic and Analytical Chemistry, Goethe University Frankfurt, Max-von-Laue Str. 7, Frankfurt am Main, 60438, Germany
[e] Deutsches Elektronen-Synchrotron DESY, Notkestr. 85, Hamburg, 22607, Germany
[f] Universite Grenoble Alpes, CNRS, Grenoble INP-UGA, SIMaP, Grenoble, F-38000, France

ARTICLE INFO

Keywords:
Modulated structure
Synchrotron radiation
Crystal-chemical analysis
Successive phase transitions
Single crystal X-ray diffraction
Mode analysis

ABSTRACT

The ferroelectric phase III of Rb_2ZnCl_4 is stable below $T_c = 192$ K. It is known to be a threefold superstructure of the centrosymmetric high-temperature structure, with space group $P2_1cn$. Below $T_L = 70$ K, phase IV exists as a sixfold superstructure. We report the crystal structure of phase IV with monoclinic symmetry Cc (b unique), while a structure model with symmetry Pn (c unique) leads to an almost equally good, yet significantly worse fit to the diffraction data. Employing the superspace approach to these commensurately modulated structures results in modulation waves that follow the two-dimensional irreducible representation T_1 of $P2_1cn$, albeit with different order parameter directions defining Cc and Pn symmetries, consistent with the literature. Standard tools of crystal-chemical analysis indicate that the sixfold superstructure is more stable than the threefold superstructure of phase III. However, crystal-chemical arguments cannot distinguish between the correct superstructure model with space group Cc (**b** unique) and the incorrect superstructure model with symmetry Pn (**c** unique) for phase IV. New crystal chemical tools are required, in order to attain a meaningful understanding of superstructure formation.

1. Introduction

Compounds A_2BX_4 (A = K, Rb, Cs; B = Zn, Co; X = Cl, Br, I) are a well studied group of materials, because of their ferroelectric properties, modulated crystal structures and successive phase transitions. Most of the compounds within the A_2BX_4 family possess the β-K_2SO_4 structure type at room temperature, which is orthorhombic with space group $Pmcn$ [1]. At high temperatures they might transform into the hexagonal α-K_2SO_4 structure type [1,2]. Other compounds in the A_2BX_4 system possess the Sr_2GeS_4 structure type with the monoclinic space group $P2_1/m$. They are often referred to as the α phase (not to be confused with hexagonal α-K_2SO_4) [2]. Compounds with the β-K_2SO_4 structure type may show complex sequences of structural phase transitions. One of the well known sequences is followed by Rb_2ZnCl_4. Rb_2ZnCl_4 has β-K_2SO_4 structure type above $T_i = 303.0$ K [Phase I; Fig. 1(a)] [3]. Below T_i, an incommensurately modulated structure develops, with temperature-dependent modulation wave vector $\mathbf{q} = (1/3\text{-}\delta)\mathbf{c}^*$ (Phase II), where δ decreases with temperature [4]. In this phase, orthorhombic symmetry is retained, while the modulation wave goes from a sinusoidal function close to T_i to a highly anharmonic function just above the lock-in transition at $T_c = 192$ K [5,6]. At T_c, δ jumps to zero, and Rb_2ZnCl_4 attains a threefold superstructure with space group $P2_1cn$ (Phase III) [4]. Again, orthorhombic symmetry is retained, but inversion symmetry is lost, such that Phase III is ferroelectric [7,8]. At $T_L = 75$ K, another phase transition involves the development of an additional, commensurate modulation, thus leading to a sixfold superstructure (Phase IV) [9]. Several other halides of A_2BX_4 (A = K, Rb; B = Zn, Co; X = Cl, Br) follow the same sequence of phase transitions [10–15].

While the modulated structures and phase transitions at T_i and T_c have been extensively studied, the phase transitions at T_L and the low temperature crystal structures have received little attention, despite

* Corresponding authors.
E-mail addresses: surya.rohith96@gmail.com (S.R. Kotla), smash@uni-bayreuth.de (S. van Smaalen).
[1] Present address; Institut NÉEL, CNRS, Univ. Grenoble Alpes, Grenoble 38000, France.

https://doi.org/10.1016/j.jssc.2025.125226
Received 14 October 2024; Received in revised form 27 December 2024; Accepted 26 January 2025
Available online 3 February 2025

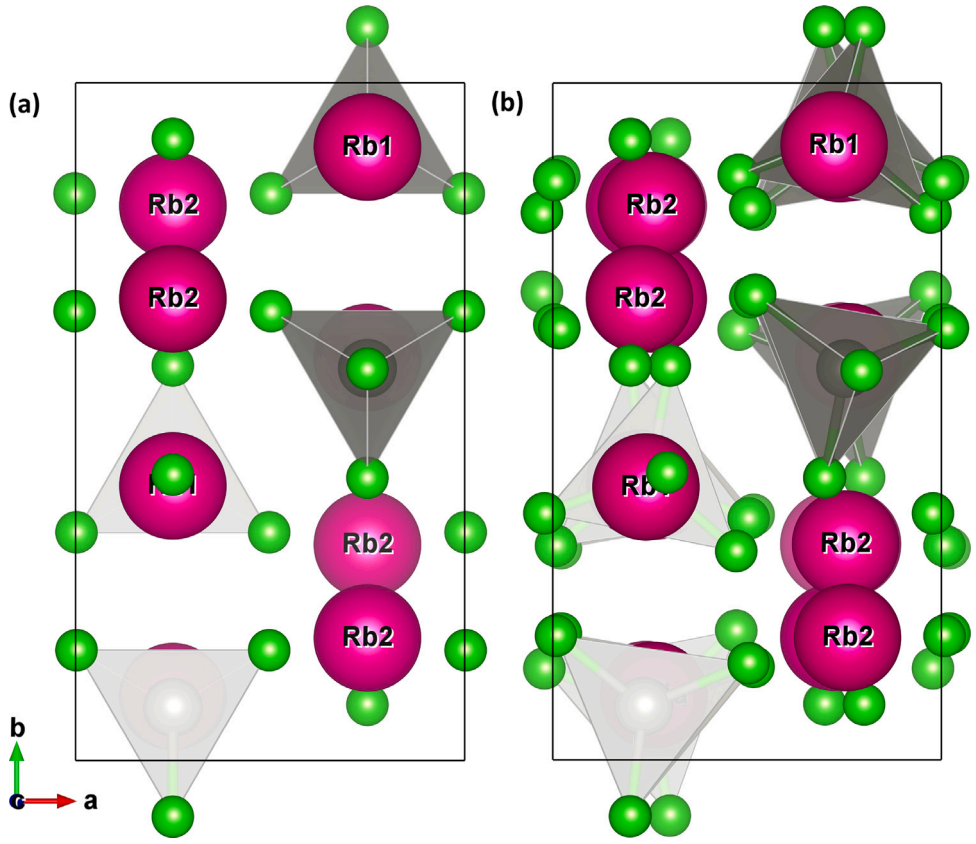

Fig. 1. Crystal structure of Rb_2ZnCl_4 projected along **c**. (a) Normal phase (Phase I) with atoms located on the mirror plane. (b) Commensurate phase (Phase III) with modulation composed of shifts of Rb atoms and rotations of $ZnCl_4$ groups.

their occurrence in several A_2BX_4 compounds. Phase IV was first discovered in Rb_2ZnCl_4 through Raman spectroscopy [16] and birefringence measurements [17]. A doubling of the unit cell was predicted with respect to the unit cell of phase III [16,17]. Subsequently, mode analysis and group-theoretical calculations indicated three possible space groups for phase IV: $C1c1$, $P11n$ and $P1$ [18]. X-ray and neutron scattering studies on Rb_2ZnCl_4 revealed additional reflections in phase IV at positions $(h+1/2, k+1/2, l)$, suggesting a doubling of unit cell within the $(\mathbf{a},\mathbf{b})$ plane. Notice that all reflection indices are given with respect to the reciprocal lattice of the basic structure of phase IV. Apart from thermal expansion and minor distortions at the phase transitions, the unit cells of the basic structures of phases II, III and IV are the same as the unit cell of phase I. From the observed reflection conditions, $C1c1$ has been suggested as the space group of the sixfold, $2a \times 2b \times 3c$ supercell [19,20]. For phase IV of K_2CoCl_4 and K_2ZnCl_4, the crystal structures have been refined with the same space group $C1c1$ of the sixfold supercell [21,22]. For other A_2BX_4 halides, like Rb_2CoCl_4 and Rb_2ZnBr_4, the same space group $C1c1$ was suggested based on the analysis of reflection conditions, but the crystal structures have not been determined [23,24]. However, a systematic approach is still lacking towards an experimental determination of the symmetry of phase IV, and towards developing an understanding of the mechanism of the phase transition. No structure solution is available for phase IV of Rb_2ZnCl_4.

The β-K_2SO_4 structure type is pseudo-hexagonal, with **c** being the pseudo-hexagonal axis of phase I (*Pmcn* setting). This direction plays an important role as it is often the direction of the modulation wave [1]. The phase transition towards the incommensurate phase II has been extensively studied, and empirical relations have been derived for understanding the I→II phase transition. The modulation in these phases mostly corresponds to rotations of the anion BX_4 tetrahedral groups about an axis almost parallel to **c** [25]. While the phase transition at T_i is accompanied by a considerable change in the lattice parameters, the lattice parameter c is usually least affected. It has been established that the size of cations and BX_4^{2-} anions play a crucial role in determining the stability of the β-K_2SO_4 structure type and the occurrence of phase transitions [26]. For small values of the ratio r_A/r_{BX}, where r_A is the radius of the cation and r_{BX} is the radius of the anion tetrahedral group, the structure is likely to undergo phase transitions. For too small values, like in the case of iodides (X = I) [27], compounds A_2BX_4 assume the Sr_2GeS_4 structure type instead of the β-K_2SO_4 structure type [23]. On the other hand, Cesium metal halides Cs_2BX_4, for which the ratio is high, follow different phase transition sequences than Rb_2ZnCl_4 [28]. Another criterion determining a transition into the incommensurate phase is provided by the bond valence sum (BVS) of the cations, A^+, as well as the bond strength of the shortest A–X bond that is almost parallel to **c** [2].

Here, we present the results of temperature-dependent single-crystal X-ray diffraction (SXRD) on Rb_2ZnCl_4 in the commensurate phase III and the low-temperature monoclinic phase IV. The space group and the crystal structure of phase IV are determined within the superspace approach. A comparison is given of the crystal structures of phases III and IV, employing established crystal-chemical concepts and criteria that have previously been applied to the phase transition I→II. These criteria show phase IV to be more stable than phase III, indeed. However, they cannot distinguish between the correct crystal structure of symmetry Cc and the incorrect crystal structure of symmetry Pn, thus failing to provide a real explanation for the stability of the structure with Cc symmetry.

2. Experimental details

2.1. Synthesis

High-quality single crystals of Rb_2ZnCl_4 have been grown from aqueous solution of stoichiometric amounts of highly pure RbCl (99.95%, Sigma-Aldrich) and $ZnCl_2$ (99.99%, Alfa Aesar) in purified water taken from a Simplicity UV by Millipore [6,8]. The solvent is slowly evaporated at 313.15 K until single crystals of appropriate sizes have been formed. The crystals are transparent and block shaped. Single crystals of approximately 0.1 mm size have been selected for the X-ray diffraction experiments.

2.2. Single-crystal X-ray diffraction

Single-crystal X-ray diffraction (SXRD) experiments have been performed at beamline P24 of PETRA-III at DESY, Hamburg, employing synchrotron radiation of wavelength 0.5000 Å. A single crystal of size $0.14 \times 0.12 \times 0.14$ mm^3 has been mounted on a four-circle Huber diffractometer. Diffraction has been measured by a Pilatus CdTe 1M detector, while continuous rotating the crystal about the ϕ axis with a speed of 1 deg/s. The diffraction was stored in frames of 0.1° wide in ϕ. The sample temperature has been controlled by a CRYOCOOL open-flow helium cryostat, employing helium as cryogas. Datasets of 3640 frames have been collected at selected temperatures, employing a sample-to-detector distance $D = 260$ mm with different attenuators and offsets of 0° and 25° in 2θ.

2.3. Data processing

The measured frames have been binned to frames of $\Delta\phi = 1°$, employing the SNBL toolbox [29]. Bragg reflections have been indexed and integrated using the EVAL15 software suite [30]. The integrated intensities have been scaled and corrected for absorption with SADABS [31], using different Laue groups as appropriate. Diffraction data have been obtained in this way for six different temperatures: 70, 80 and 90 K for phase III, and 20, 40 and 60 K for phase IV. Structure refinements have been performed with JANA2020 [32]. Reciprocal-space images have been created with CrysAlis^{Pro} [33].

3. Results

With reference to the lattice parameters of phase I, the commensurately modulated crystal structure of phase III can be considered as a threefold, $a \times b \times 3c$ superstructure with space group $P2_1cn$ (Table 1) [4,7,34]. Strong superlattice reflections are visible along l in the reconstructed $(h\,1\,l)$ reciprocal lattice plane for the 90 K SXRD data [Fig. 2(b)]. Fig. 2(b) also shows weak diffuse streaks between the Bragg reflections along $\mathbf{c}^*$. These streaks remain present in phase IV. Therefore, they are not related to the development of the $\mathbf{q}^2$ modulation. Instead, they might be the result of imperfections within the $\mathbf{q}^1$ modulation wave.

The superspace approach to phase III employs the lattice parameters a, b and c for the basic structure in combination with the commensurate modulation wave vector $\mathbf{q} = (1/3)\,\mathbf{c}^*$ and the orthorhombic superspace group $Pmcn(00\gamma)ss0$ (Table 1). This is the same superspace group as is valid for the incommensurate phase II. Unlike the incommensurate case, the phase of the modulation, t, needs to be specified for the commensurate structures [36,37]. In the present case it is determined as $t_0 = 1/4$. The basic structure comprises six independent atoms: Rb1, Rb2, Zn, Cl1, Cl2 and Cl3. The commensurately modulated structure furthermore involves up to third-order harmonic parameters for displacement modulation and for modulation of the atomic displacement parameters (ADPs). Refinements resulted in an excellent fit to the SXRD data with $R_F(m = 0) = 2.92\%$ for main reflections and $R_F(m = 1) = 1.98\%$ for satellite reflections (Table 1). See Tables S4–S7 in the Supplemental Information for the values of the atomic coordinates and modulation amplitudes. The superspace structure model has been transformed into the supercell model (Table 1). See Table S8 in the Supplemental Information for the values of the atomic coordinates with respect to the threefold supercell. From the refined modulation amplitudes it became clear that major part of the modulation are rotations of the $ZnCl_4$ tetrahedral groups about an axis within the mirror plane, almost parallel to the **c**-axis. In the case of Rb atoms the modulation is mostly in the direction perpendicular to the mirror plane, *i.e.* along **a**. The Zn atoms have the smallest modulation amplitudes. These results are in good agreement with the literature [7,34]. They can be visualized in a projection of the crystal structure along **c** [Fig. 1(b)].

The low-temperature phase IV is defined by the presence of additional superlattice reflections below $T_L \approx 70$ K [19]. In the present SXRD data they appear as diffuse signatures at 70 K, while they are sharp Bragg reflections at positions $(1/2)\mathbf{a}^* + (1/2)\mathbf{b}^*$ at 60 K and below (Fig. 2). These satellite reflections are visible not only at $(h/2, k/2, l)$, but also at $(h/2, k/2, l \pm 1/3)$, where reflection indices refer to the basic-structure unit cell. Based on the observed reflection conditions in their diffraction patterns of Rb_2ZnCl_4, several space groups have been

Table 1
Crystallographic information of Rb_2ZnCl_4 at 90 K (commensurate phase) and 40 K (LT phase).

Temperature (K)	90	40
Crystal system	Orthorhombic	Monoclinic
Superspace group	$Pmcn(00\gamma)ss0$	$Pc(\alpha 0\gamma)s(1/2\beta 0)0$
No. [35]	62.1.9.6	7.2.12.7
a (Å)	7.22619(8)	7.22614(8)
b (Å)	12.60031(14)	12.57385(12)
c (Å)	9.17959(4)	9.16979(9)
Volume (Å^3)	835.823(16)	833.171(15)
Wavevector **q1**	$\frac{1}{3}\mathbf{c}^*$	$\frac{1}{3}\mathbf{c}^*$
Wavevector **q2**	–	$\frac{1}{2}\mathbf{a}^* + \frac{1}{2}\mathbf{b}^*$
Z	4	4
Wavelength (Å)	0.50000	0.50000
Detector distance (mm)	260	260
2θ-offset (deg)	0, 27.6	0, 25
χ-offset (deg)	−60	−60
Rotation per image (deg)	0.1	0.1
$(\sin(\theta)/\lambda)_{max}$ (Å^{-1})	0.777011	0.734722
Absorption, μ (mm^{-1})	6.140	6.159
T_{min}, T_{max}	0.4152, 0.5379	0.4584, 0.5297
Criterion of observability	$I > 3\sigma(I)$	$I > 3\sigma(I)$
No. of reflections measured,		
$(m = 0, 0)$	3602	3367
$(m = 1, 0)$	7483	6840
$(m = 0, 1)$	–	3527
$(m = 1, 1)$	–	6937
Unique reflections (obs/all),		
$(m = 0, 0)$	1123/1326	1497/1810
$(m = 1, 0)$	1341/2681	1912/3620
$(m = 0, 1)$	–	865/2485
$(m = 1, 1)$	–	1477/4897
R_{int} $(m = 0, 0)$ (obs/all)	0.0497/0.0498	0.0342/0.0343
R_{int} $(m = 1, 0)$ (obs/all)	0.0327/0.0368	0.0308/0.0334
R_{int} $(m = 0, 1)$ (obs/all)	–	0.0339/0.0386
R_{int} $(m = 1, 1)$ (obs/all)	–	0.0476/0.0529
No. of parameters	190	569
R_F $(m = 0, 0)$ (obs)	0.0292	0.0300
R_F $(m = 1, 0)$ (obs)	0.0198	0.0256
R_F $(m = 0, 1)$ (obs)	–	0.0279
R_F $(m = 1, 1)$ (obs)	–	0.0295
wR_F all (all)	0.0389	0.0425
GoF (obs/all)	1.31/1.02	0.99/0.70
Supercell description		
Space group	$P2_1cn$	$C1c1$
a (Å)	7.22619(8)	14.45228(16)
b (Å)	12.60031(14)	25.1477(24)
c (Å)	27.53877(12)	27.50937(27)
Z	12	48
Unique reflections (obs/all)	2464/4007	5599/10873
R_F(obs)	0.0261	0.0283
wR_F(all)	0.0389	0.0422

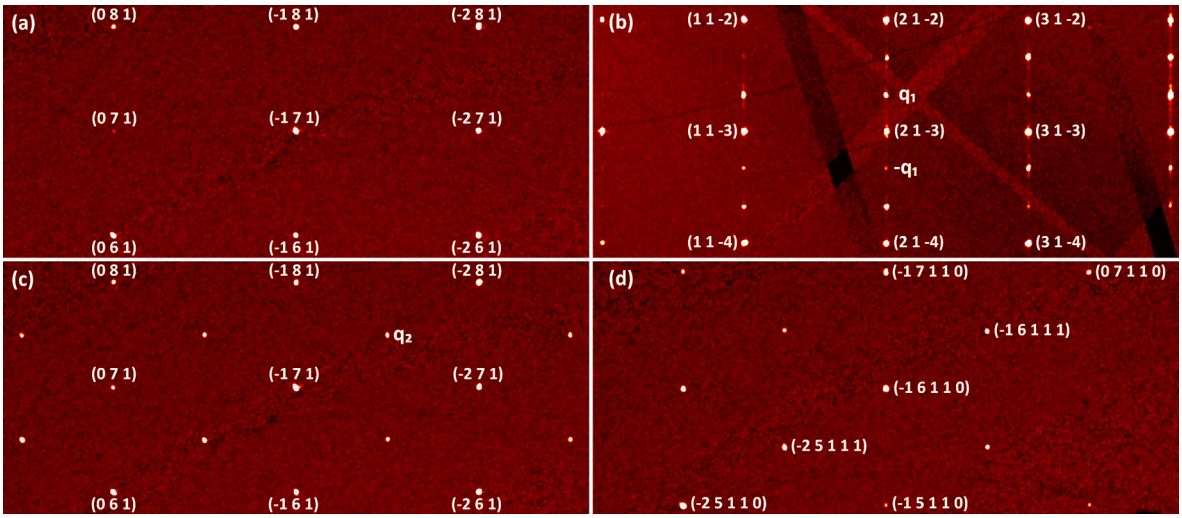

Fig. 2. Unwarp images of reciprocal space (a) ($h\,k\,1$) and (b) ($h\,1\,l$) layers at 90 K. (c) ($h\,k\,1$) layer at 40 K; unindexed reflections are satellites. (d) ($h\,k$ 1.33) layer at 40 K, where reflections are indexed in (3 + 2)D space, so that mixed satellites $q^1 + q^2$ can be observed.

proposed for the $2a \times 2b \times 3c$ supercell [7,16,20], but none of them has been confirmed by a structure solution.

The crystal structure of phase IV can be described within the superspace approach, employing the same basic structure as phase III, but with two modulation waves instead of one wave,

$$\mathbf{q}^1 = \tfrac{1}{3}\mathbf{c}^* \qquad \mathbf{q}^2 = \tfrac{1}{2}\mathbf{a}^* + \tfrac{1}{2}\mathbf{b}^* . \tag{1}$$

Symmetry analysis revealed that the orthorhombic symmetry of the basic structure, *Pmcn*, is incompatible with the commensurate modulation $\mathbf{q}^2$. Specifically, the twofold commensurability of $\mathbf{q}^2$ implies the loss of the 2_1 screw axes along **a** and **b**. As a result, the two-dimensionally (2D) modulated crystal structure of phase IV can only be described by a monoclinic or triclinic superspace group. The space group of the sixfold supercell is monoclinic or triclinic, accordingly.

Nevertheless, no peak splitting nor other signatures of loss of orthorhombic lattice symmetry are visible in the present SXRD data, consistent with earlier XRD experiments on Rb_2ZnCl_4 and related compounds [19,21–23]. Moreover, structure refinements of the $\mathbf{q}^1$-modulated crystal structure of symmetry $Pmcn(00\gamma)ss0$ against SXRD data of phase IV resulted in an excellent fit to the main reflections and first-order $\mathbf{q}^1$ satellite reflections (model "only q1" in Table 2). These results imply that the basic structure and the $\mathbf{q}^1$ modulation retain orthorhombic symmetry, and symmetry breaking is entirely due to the $\mathbf{q}^2$ modulation. As a consequence, it appeared necessary to introduce the orthorhombic restrictions of the $\mathbf{q}^1$ modulation as additional, non-symmetry restrictions into the refinements of monoclinic structure models for phase IV. A similar situation has been encountered for Mo_2S_3, where a monoclinic basic structure is combined with one modulation wave that preserves monoclinic symmetry, while the second modulation wave enforces triclinic symmetry [38]. Structure refinements have been performed against the 40 K SXRD data for structure models according to each of the possible monoclinic superspace groups, *i.e.* those monoclinic superspace groups that are based on monoclinic space groups that are subgroups of *Pmcn*. A total of twelve different structure models have thus been tested, and their fits to the SXRD data are compared in Table S1 of the Supplementary Information. The best fit to the 40 K SXRD data was achieved by a structure model with the superspace group $P1c1(\alpha 0\gamma)s(1/2\beta 0)0$ and commensurate phases $t_0 = 1/4$ and $u_0 = 1/8$. Within the superstructure description, this model corresponds to a 6-fold, $2a \times 2b \times 3c$ supercell with space group $C1c1$. Therefore, we refer to this model as "model *Cc*" (Table 2).

A very good, yet significantly worse fit to the 40 K SXRD data was achieved by a structure model with the superspace group $P11n(00\gamma)0(\alpha\beta 0)0$ and commensurate phases $t_0 = 1/4$, $u_0 = 0$. In this case, the 6-fold, $2a \times 2b \times 3c$ supercell has a space group with the tentative symbol $C11d$ [39]. Space group $C11d$ is a non-standard, pseudo-orthorhombic setting of space group *Pn*. Therefore, this model is referred to as "model *Pn*" (Table 2). It should be noticed that reflection conditions are fulfilled by the present SXRD data for both the *Cc* and *Pn* models. The two structure models have also been refined against the SXRD data averaged in Laue symmetry *mmm*. In this case, *Pn* and *Cc* employ identical data sets. The results still favor model *Cc* (Table S2 in the Supplemental Material). Furthermore, it has been reported that a spontaneous dielectric polarization develops along **c** below T_L, which is incompatible with *Pn* [40]. Therefore, all evidence points towards model *Cc* as the correct structure model for Phase IV. Characteristic parameters of the superspace refinement and the 6-fold, $2a \times 2b \times 3c$ supercell lattice are presented in Table 1. A total of 569 parameters are used in the refinement as opposed to 753 parameters for supercell refinements of K_2CoCl_4 and K_2ZnCl_4 [21,22]. The smaller number of parameters is the result of the superspace approach as opposed to a supercell refinement.

Both structure models *Cc* and *Pn* for phase IV employ the same basic-structure parameters and $\mathbf{q}^1$-modulation parameters as have been

Table 2
Structure refinements against SXRD data at 40 K for three structure models ("only q1," Cc and Pn). "Only q1" has inversion twinning with restricted twin volume fractions of 0.5. *Cc* and *Pn* models each have four domains defined by the identity, a twofold rotation about **a**, the inversion center, and a mirror perpendicular to **a**. Volume fractions of domains 1 and 3 are equal, and those of domains 2 and 4 are equal to each other too. The row 'twin volume fraction' gives the volume fractions of domains 1 and 2.

Model	Only q1	*Cc*	*Pn*
Superspace group	$Pmcn(00\gamma)ss0$	$P1c1(\alpha 0\gamma)s(1/2\beta 0)0$	$P11n(00\gamma)0(\alpha\beta 0)0$
Modulation phases	t_0=1/4	t_0=1/4, u_0=1/8	t_0=1/4, u_0=0
Point group for averaging	*mmm*	12/*m*1	112/*m*
Unique reflections (obs/all)	2344/3673	5751/12812	6072/13320
Main (obs/all)	1001/1241	1497/1810	1610/1980
Sat (1,0) (obs/all)	1343/2432	1912/3620	1988/3989
Sat (0,1) (obs/all)	–	865/2485	913/2520
Sat (1,1) (obs/all)	–	1477/4897	1561/4831
R_{int} (obs/all) %	3.82/3.92	3.41/3.48	3.51/3.61
No. of Parameters	190	569	569
R_{obs} %	2.86	2.86	3.13
R_{obs}(main)%	2.86	3.00	3.25
R_{obs}(1,0 sat)%	2.85	2.56	2.71
R_{obs}(0,1 sat)%	–	2.79	3.10
R_{obs}(1,1 sat)%	–	2.95	3.52
twin volume fraction	0.5	0.228/0.272	0.247/0.253

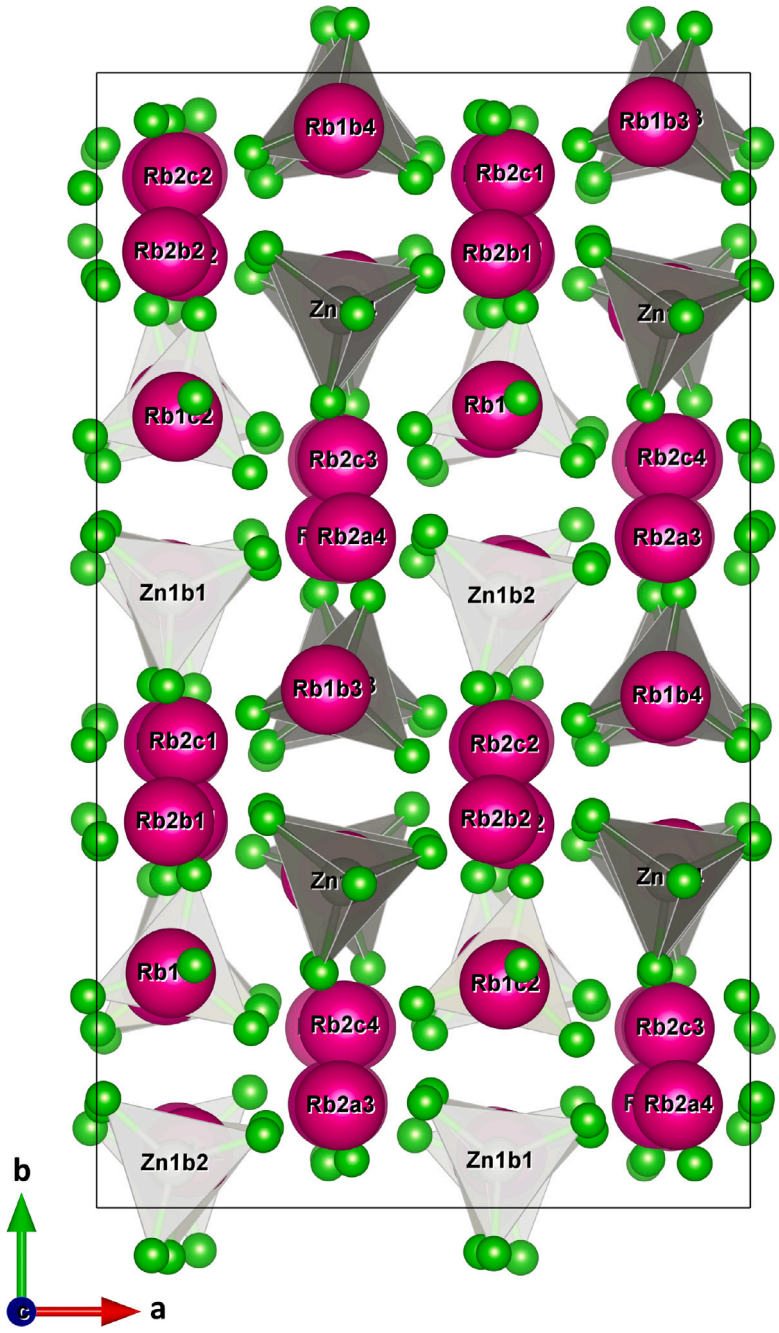

Fig. 3. Supercell of model *Cc* for the low-temperature phase IV at 40 K, projected along **c**.

used for phase III. Even the numerical values of these parameters are similar for phases III and IV (compare Tables S7 and S11 in the Supplemental Material). In addition to those parameters, modulation functions have been used for phase IV according to the $\mathbf{q}^2$ and $(\mathbf{q}^1+\mathbf{q}^2)$ harmonic waves. The refined modulation parameters indicate that the $\mathbf{q}^1$ modulation is much larger than the $\mathbf{q}^2$ modulation (Tables S11–S12 in the Supplemental Material). This feature is reflected in the diffraction pattern, as the $\mathbf{q}^1$ satellites are almost ten times stronger than the $\mathbf{q}^2$ satellites. The mixed, $(\mathbf{q}^1+\mathbf{q}^2)$ satellites are stronger than the $\mathbf{q}^2$ satellites, but they are weaker than the $\mathbf{q}^1$ satellites. Therefore, the modulation in phase IV is dominated by the $\mathbf{q}^1$ modulation, while the $\mathbf{q}^2$ modulation is responsible for a relatively small correction (Fig. 3).

4. Discussion

Crystal structures in general are rationalized on the basis of several types of structural parameters, including bond lengths, bond angles, non-bonded contacts, coordination numbers, the calculated valence according to the bond-valence method [41] and the distortion index for tetrahedral groups [42]. Here, we will apply these methods to different structure models for phase IV: the basic structure, the "only q1" model and the models *Cc* and *Pn* (Table 2). Furthermore, we include phase III into the analysis, whereby the "only q1" model for phase IV employs the same parameters as the modulated structure of phase III. We will show that the additional modulation of phase IV leads to a more favorable crystal structure than that of phase III (than the "only q1" model) by all criteria as discussed in the literature

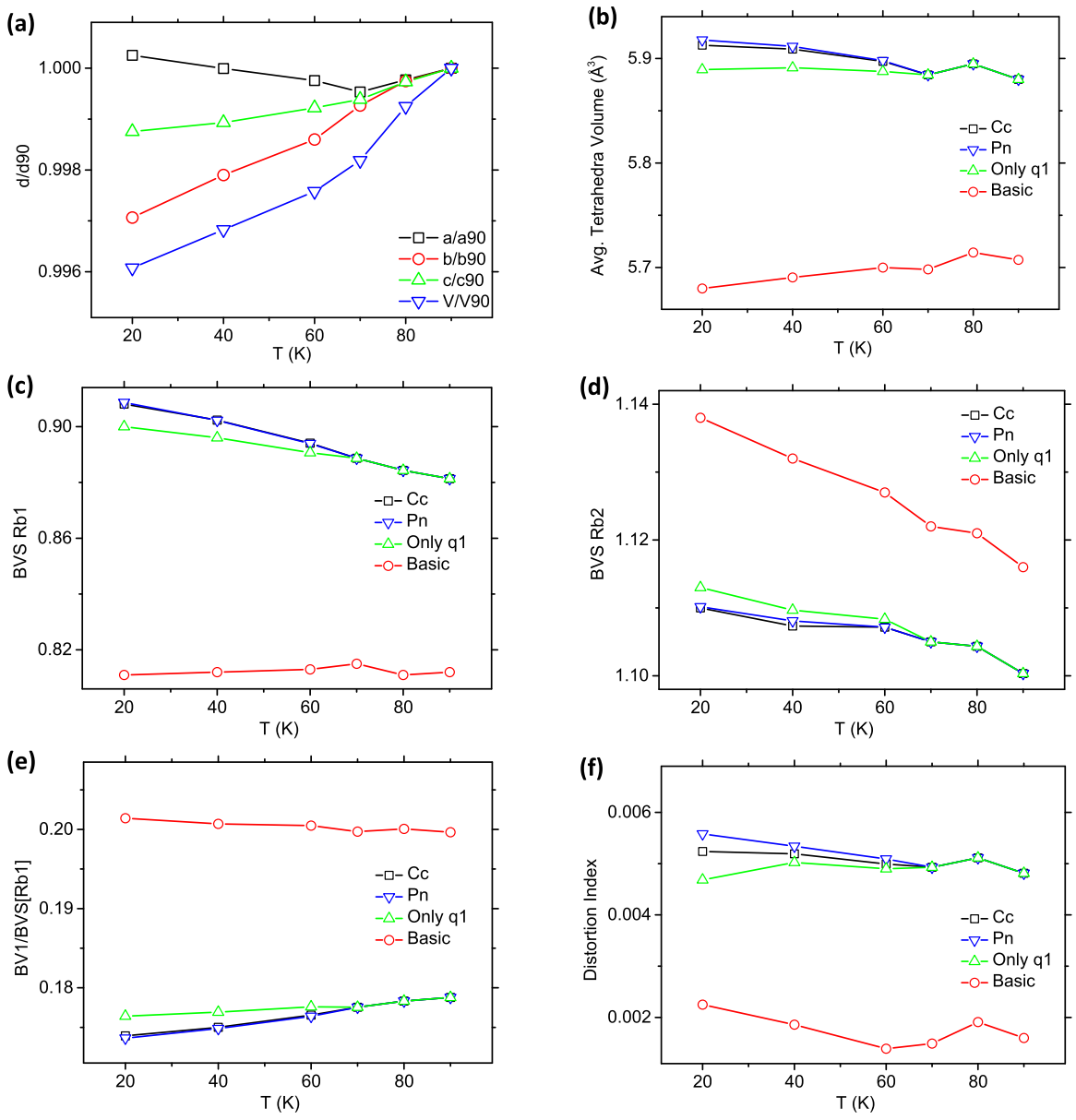

Fig. 4. Temperature dependence of several structural parameters for four different structure models. (a) Lattice parameters. (b) Average Tetrahedra volume. (c) Bond Valence Sum (BVS) for Rb1. (d) Bond Valence Sum (BVS) for Rb2. (e) Ratio BV1/BVS[Rb1]. (f) Tetrahedron Distortion Index.

[2,21,22,42]. However, none of these criteria can distinguish between models *Cc* and *Pn*. The thermal evolution about $T_L \approx 70$ K will be evaluated by comparing with each other the crystal structures of phase IV at 20, 40 and 60 K, and of phase III at 70, 80 and 90 K (Tables S2 and S3 in Supplemental Material).

Rb_2ZnCl_4 exhibits a conventional thermal expansion for the temperature range 20–90 K across the phase transition at T_L [Fig. 4(a)], consistent with earlier reports [19]. Exception is the linear expansion along **a**, where *a* attains a minimum value near T_L. This signature of the phase transition III→IV might be related to the volume of the $ZnCl_4$ tetrahedral groups, which starts to increase upon cooling below T_L [Fig. 4(b)].

The periodic phase (Phase I) of the compounds A_2BX_4 with the β-K_2SO_4 structure type has two crystallographically independent A atoms. Specifically for Rb_2ZnCl_4, the atom Rb1 is in 11-fold and Rb2 in 9-fold coordination by Cl [Fig. 1(a)]. Typical for the compounds A_2BX_4 is that Rb1 is underbonded and Rb2 is overbonded [2]. We have analyzed the present crystal structures by computation of the valences of Rb1 and Rb2 according to the Bond Valence Method [41,43,44]. The average bond valence sum (BVS) of Rb1 in the basic structure is about 0.81 and the BVS of Rb2 is 1.12 [Fig. 4(c,d)]. For the modulated structure of phase III as well as for the corresponding model "only q1" for phase IV, the BVS of Rb1 is increased towards 0.88 and higher, while the BVS of overbonded Rb2 is decreased towards 1.10 [Fig. 4(c,d)]. The partial relieve of the underbonded/overbonded character might be a driving force towards the development of the $\mathbf{q}^1$-type modulation. The stability of the $\mathbf{q}^2$-type modulation in phase IV then is explained by the additional modifications of the BVSs into the direction of valence 1, as it is the case for both models *Cc* and *Pn*. However, the effect on the BVS of the $\mathbf{q}^1$-type modulation is much larger than that of the $\mathbf{q}^2$-type modulation, explaining why the latter develops at lower temperatures than the former.

It was suggested by Fabry and Peréz-Mato [2] that the value of the BVS of underbonded A1 is not a conclusive criterion for rationalizing the development of the $\mathbf{q}^1$-type modulation. In addition, they considered the shortest Rb1–Cl contact, which is the Rb1–Cl bond parallel to **c**, and which contributes BV1 to the BVS of Rb1. They proposed that a transition I→II will take place, if the ratio BV1/BVS[Rb1] exceeds

the value 0.24. Extending this argument to the other phase transitions, we presently observe that BV1/BVS[Rb1] decreases – *i.e.* a more stable structure forms – upon introduction of the $\mathbf{q}^1$-type modulation and it further decreases with the $\mathbf{q}^2$-type modulation [Fig. 4(e)]. Again, models *Cc* and *Pn* cannot be distinguished by this criterion.

Major part of the modulation is rotations of the $ZnCl_4$ tetrahedral groups. The basic structure contains one crystallographically independent $ZnCl_4$ group. In phase III and for model "only q1" for phase IV, the threefold supercell contains three independent groups. The 6-fold supercell together with loss of point symmetry then leads to 12 independent $ZnCl_4$ tetrahedral groups in the supercell of models *Cc* and *Pn*. For the basic structure we already find that the $ZnCl_4$ tetrahedral group is distorted, as exemplified by the distortion index [Fig. 4(f)], and the variation of bond angles within the range 105.9°–114.7°. Both $\mathbf{q}^1$-type and $\mathbf{q}^2$-type modulations are responsible for an increase of the distortion [Fig. 4(f)]. Nevertheless, the average bond angle is 109.4°, close to the value of a regular tetrahedron. We have not been able to determine, whether or not these distortions represent a favorable structural feature.

A further attempt has been made to distinguish models *Cc* and *Pn* by key structural characteristics. Specifically, average bond lengths and their variances have been computed for the coordinations of each of the twelve independent Rb1, Rb2 and Zn atoms (Tables S16–S33 in the Supplemental Material). However, models *Cc* and *Pn* again follow the same trend. In this respect it should be noticed that the models '*Cc*' and '*Pn*' can be described by exactly the same list of 84 independent atoms in the supercell. Difference is the long-range order, as it is implied by the different symmetries. Furthermore, differences exist for the spatial arrangements of the bonds in their coordination polyhedra. However, as mentioned above, leading to the same average values and their variances.

The phase transition III → IV involves a doubly degenerate soft mode at the *T*-point (−1/2, 1/2, 0) of the Brillouin zone of the space group $P2_1cn$ of the supercell for phase III [20]. Both *Cc* and *Pn* symmetries are the result of distortions following the same, two-dimensional irreducible representation (irrep), T_1, of $P2_1cn$, consistent with earlier reports [18]. Employing the ISOTROPY software [45,46] to the present *Cc* structure model for phase IV, results in a primary distortion with order parameter direction (OPD) (0,a) and amplitude 1.4313 Å. Secondary modes are Γ_1 and Γ_4, which are found to possess negligible amplitudes. The *Pn* structure maps onto OPD (a,a) with amplitude 1.4306 Å. Here, secondary modes are Γ_1 and Γ_3, again with negligible amplitudes. The good fit to the diffraction data of phase IV of both *Cc* and *Pn* models is probably the result of the similar distortions in conjunction with the twinned data.

However, the observations from standard methods of crystal chemical analysis conclude that they are insufficient for explaining the stability of model *Cc* over model *Pn*. Other tools are thus required for distinguishing different models for the modulated structures of Rb_2ZnCl_4. Calculation of the electronic structures by Density Functional Theory (DFT) might lead to different stabilities of the *Cc* and *Pn* structure models. However, such calculations are challenging for 84 independent atoms in the large supercell, and they are beyond the scope of the present work.

5. Conclusions

The low-temperature threefold and sixfold superstructures of Rb_2ZnCl_4 have been refined against SXRD data, employing the superspace approach. The crystal structure of the lock-in phase III has the orthorhombic superspace group $Pmcn(00\gamma)ss0$. The commensurate modulation with $\mathbf{q}^1 = (0, 0, 1/3)$ corresponds to a threefold $a \times b \times 3c$ supercell with space group $P2_1cn$ [4]. The superspace approach to the second modulation with $\mathbf{q}^2 = (1/2, 1/2, 0)$ implies a reduction of symmetry towards monoclinic. We have found the (3 + 2)-dimensional superspace group $Pc(\alpha 0\gamma)s(1/2\beta 0)0$, which leads to a $2a \times 2b \times 3c$ supercell with symmetry $C1c1$. An almost equally good, yet significantly worse fit to the diffraction data has been obtained for a model with superspace group $P11n(00\gamma)0(\alpha\beta 0)0$, corresponding to space group $C11d$ (standard setting Pn) for the $2a \times 2b \times 3c$ supercell. Evaluation of several crystal parameters, like the BVS, demonstrates that the structure is stabilized by the $\mathbf{q}^1$-type modulation and it is further stabilized by the additional $\mathbf{q}^2$-type modulation. None of the crystal-chemical criteria can distinguish between models *Cc* and *Pn* for Rb_2ZnCl_4. Other tools are thus required for a crystal-chemical rationalization of superstructures.

CRediT authorship contribution statement

Surya Rohith Kotla: Writing – original draft, Methodology, Investigation, Formal analysis, Data curation, Conceptualization. **Sitaram Ramakrishnan:** Writing – review & editing, Investigation, Data curation. **Achim M. Schaller:** Writing – review & editing, Data curation. **Toms Rekis:** Writing – review & editing, Data curation. **Claudio Eisele:** Writing – review & editing, Data curation. **Jin-Ke Bao:** Writing – review & editing, Data curation. **Leila Noohinejad:** Writing – review & editing, Software, Resources, Data curation. **Geoffroy de Laitre:** Writing – review & editing, Investigation. **Marc de Boissieu:** Writing – review & editing, Methodology, Conceptualization. **Sander van Smaalen:** Writing – review & editing, Supervision, Resources, Project administration, Methodology, Investigation, Funding acquisition, Conceptualization.

Declaration of competing interest

The authors declare that they have no known competing financial interests or personal relationships that could have appeared to influence the work reported in this paper.

Acknowledgments

High-quality single crystals of Rb_2ZnCl_4 were grown by Kerstin Küspert at the Laboratory of Crystallography in Bayreuth. We thank Franz Fischer for technical assistance. We acknowledge DESY (Hamburg, Germany), a member of the Helmholtz Association HGF, for the provision of experimental facilities. Parts of this research were carried out at PETRA III, using beamline P24. Beamtime was allocated for proposal I-20190544. We thank Martin Tolkiehn and Carsten Paulmann for their support of our experiment at beamline P24. This research has been funded by the Deutsche Forschungsgemeinschaft (DFG, German Research Foundation) – 406658237.

Appendix A. Supplementary data

Supplementary material related to this article can be found online at https://doi.org/10.1016/j.jssc.2025.125226.

Data availability

Data will be made available on request.

References

[1] H.Z. Cummins, Experimental studies of structurally incommensurate crystal phases, Phys. Rep. 185 (1990) 211–409, http://dx.doi.org/10.1016/0370-1573(90)90058-A.

[2] J. Fabry, J.M. Perez-Mato, Some stereochemical criteria concerning the structural stability of A_2BX_4 compounds of type β-K_2SO_4, Phase Transit. 49 (1994) 193–229, http://dx.doi.org/10.1080/01411599408201174.

[3] K. Itoh, A. Hinasada, H. Matsunaga, E. Nakamura, Disordered structure of Rb_2ZnCl_4 in the normal phase, J. Phys. Soc. Japan 52 (1983) 664–670, http://dx.doi.org/10.1143/JPSJ.52.664.

[4] K. Gesi, M. Iizumi, Neutron scattering study on the incommensurate phases in ferroelectric Rb_2ZnCl_4 and K_2ZnCl_4, J. Phys. Soc. Japan 46 (1979) 697–698, http://dx.doi.org/10.1143/JPSJ.46.697.

[5] I. Aramburu, K. Friese, J.M. Perez-Mato, W. Morgenroth, M. Aroyo, T. Breczewski, G. Madariaga, Modulated structure of Rb_2ZnCl_4 in the soliton regime close to the lock-in phase transition, Phys. Rev. B 73 (2006) 014112, http://dx.doi.org/10.1103/PhysRevB.73.014112.

[6] L. Li, A. Wolfel, A. Schonleber, S. Mondal, A.M.M. Schreurs, L.M.J. Kroon-Batenburg, S. van Smaalen, Modulated anharmonic ADPs are intrinsic to aperiodic crystals: a case study on incommensurate Rb_2ZnCl_4, Acta Crystallogr. B 67 (2011) 205–217, http://dx.doi.org/10.1107/S0108768111013814.

[7] M. Quilichini, J. Pannetier, Neutron structural study of the successive phase transitions in Rb_2ZnCl_4, Acta Crystallogr. B 39 (1983) 657–663, http://dx.doi.org/10.1107/S0108768183003183.

[8] S. Sawada, Y. Shiroishi, A. Yamamoto, M. Takashige, M. Matsuo, Ferroelectricity in Rb_2ZnCl_4, J. Phys. Soc. Japan 43 (1977) 2099–2100, http://dx.doi.org/10.1143/JPSJ.43.2099.

[9] E. Francke, M. Le Postollec, J.P. Mathieu, H. Poulet, Evidence for a new phase transition in Rb_2ZnCl_4 by raman scattering, Solid State Commun. 33 (1980) 155–156, http://dx.doi.org/10.1016/0038-1098(80)90720-6.

[10] H. Mashiyama, H. Suzuki, F. Shimizu, T. Yamaguchi, S. Sawada, X-ray study on the successive phase transitions of K_2CoCl_4, J. Phys. Soc. Japan 59 (1990) 3479–3482, http://dx.doi.org/10.1143/JPSJ.59.3479.

[11] K. Gesi, Dielectric, calorimetric, and neutron diffraction studies of the phase transition in K_2ZnCl_4 at 145 K, J. Phys. Soc. Japan 61 (1992) 1225–1231, http://dx.doi.org/10.1143/JPSJ.61.1225.

[12] K. Gesi, Dielectric evidence for low temperature phase transitions in ferroelectric Rb_2CoCl_4 and Rb_2CoBr_4 crystals, J. Phys. Soc. Japan 54 (1985) 2401–2403, http://dx.doi.org/10.1143/JPSJ.54.2401.

[13] H. Kasano, H. Mashiyama, K. Gesi, K. Hasebe, X-ray study on phase transitions in ferroelectric Rb_2CoX_4 (X=Cl or Br) crystal, J. Phys. Soc. Japan 56 (1987) 831–832, http://dx.doi.org/10.1143/JPSJ.56.831.

[14] H. Mashiyama, H. Kasano, T. Yamaguchi, Incommensurate-commensurate transition in K_2ZnBr_4 and K_2CoBr_4, J. Phys. Soc. Japan 60 (1991) 45–48, http://dx.doi.org/10.1143/JPSJ.60.45.

[15] T. Yamaguchi, S. Sawada, Ferroelectricity along the a- and c-directionswith antiferroelectricity along the b-directionin Rb_2ZnBr_4 and Rb_2CoBr_4, J. Phys. Soc. Japan 60 (1991) 3162–3166, http://dx.doi.org/10.1143/JPSJ.60.3162.

[16] M. Wada, A. Sawada, Y. Ishibashi, Experimental study of the low temperature phase transition of Rb_2ZnCl_4, J. Phys. Soc. Japan 50 (1981) 531–537, http://dx.doi.org/10.1143/JPSJ.50.531.

[17] P. Günter, R. Sanctuary, F. Rohner, H. Arend, W. Seidenbusch, Evidence for low temperature phase transition in Rb_2ZnCl_4 from dielectric constant and birefringence measurements, Solid State Commun. 37 (1981) 883–888, http://dx.doi.org/10.1016/0038-1098(81)90502-0.

[18] V. Dvorak, R. Kind, On the low-temperature phase in Rb_2ZnCl_4, Phys. Status Solidi (B) 107 (1981) K109–K113, http://dx.doi.org/10.1002/pssb.2221070253.

[19] B.S. Bagautdinov, V.S. Shekhtman, Evolution of the structure of Rb_2ZnCl_4 over the temperature range 4.2–310 K, Phys. Solid State. 41 (1999) 987–993, http://dx.doi.org/10.1134/1.1130929.

[20] H. Mashiyama, K. Sugimoto, Y. Oohara, H. Yoshizawa, Neutron scattering study on phase transition at 74 K in Rb_2ZnCl_4, J. Phys. Soc. Japan 61 (1992) 3042–3045, http://dx.doi.org/10.1143/JPSJ.61.3042.

[21] H. Mashiyama, A structural study of the commensurate-commensurate transition in K_2CoCl_4 at 142 K, J. Phys. Soc. Japan 60 (1991) 180–187, http://dx.doi.org/10.1143/JPSJ.60.180.

[22] H. Mashiyama, Low-temperature commensurate phase of potassium tetrachlorozincate, K_2ZnCl_4, Acta Crystall. Sect. C 49 (1993) 9–12, http://dx.doi.org/10.1107/S010827019200547X.

[23] H. Shigematsu, K. Nishiyama, Y. Kawamura, H. Mashiyama, Neutron and x-ray scattering studies of Rb_2CoCl_4 and successive phase transition in A_2BX_4-type crystals, J. Phys. Soc. Japan 83 (2014) 124601, http://dx.doi.org/10.7566/JPSJ.83.124601.

[24] H. Shigematsu, H. Mashiyama, Y. Oohara, K. Ohshima, Neutron and X-ray scattering studies of structural phase transitions and soft modes in Rb_2ZnBr_4, J. Phys.: Condens. Matter. 10 (1998) 5861, http://dx.doi.org/10.1088/0953-8984/10/26/014.

[25] M. Iizumi, J.D. Axe, G. Shirane, K. Shimaoka, Structural phase transformation in K_2SeO_4, Phys. Rev. B 15 (1977) 4392–4411, http://dx.doi.org/10.1103/PhysRevB.15.4392.

[26] I. Etxebarria, J.M. Perez-Mato, G. Madariaga, Lattice dynamics, structural stability, and phase transitions in incommensurate and commensurate A_2BX_4 materials, Phys. Rev. B 46 (1992) 2764–2774, http://dx.doi.org/10.1103/PhysRevB.46.2764.

[27] K. Geshi, Phase transitions in monoclinic rubidium tetraiodozincate Rb_2ZnI_4, J. Phys. Soc. Japan 53 (1984) 3850–3854, http://dx.doi.org/10.1143/JPSJ.53.3850.

[28] R. Puget, M. Jannin, R. Perret, L. Godefroy, G. Godefroy, Crystallographic study of a family of Cs_2BX_4 compounds, Ferroelectrics 107 (1990) 229–234, http://dx.doi.org/10.1080/00150199008221543.

[29] V. Dyadkin, P. Pattison, V. Dmitriev, D. Chernyshov, A new multipurpose diffractometer PILATUS@SNBL, J. Synchrotron Radiat. 23 (2016) 825–829, http://dx.doi.org/10.1107/S1600577516002411.

[30] A.M.M. Schreurs, X. Xian, L.M.J. Kroon-Batenburg, EVAL15: a diffraction data integration method based on ab initio predicted profiles, J. Appl. Crystallogr. 43 (2010) 70–82, http://dx.doi.org/10.1107/S0021889809043234.

[31] G.M. Sheldrick, SADABS, Version 2008/1, University of Göttingen, Göttingen, 2008.

[32] V. Petricek, M. Dusek, L. Palatinus, Crystallographic computing system JANA2006: general features, Z. Kristallogr. 229 (2014) 345–352, http://dx.doi.org/10.1515/zkri-2014-1737.

[33] CrysAlis PRO, Yarnton, Oxfordshire, Agilent, England, 2014.

[34] K. Itoh, A. Hinasada, M. Daiki, E. Nakamura, Crystal structure of Rb_2ZnCl_4 in the modulated phases, J. Phys. Soc. Japan 58 (1989) 2070–2074, http://dx.doi.org/10.1143/JPSJ.58.2070.

[35] H.T. Stokes, B.J. Campbell, S. van Smaalen, Generation of $(3+d)$-dimensional superspace groups for describing the symmetry of modulated crystalline structures, Acta Crystallogr. A 67 (2011) 45–55, http://dx.doi.org/10.1107/S0108767310042297.

[36] S. van Smaalen, Incommensurate Crystallography, Oxford University Press, Oxford, 2012.

[37] S. van Smaalen, An elementary introduction to superspace crystallography, Z. Kristallogr. 219 (2004) 681–691.

[38] W.J. Schutte, F. Disselborg, J.L. de Boer, Determination of the two-dimensional incommensurately modulated structure of Mo_2S_3, Acta Crystallogr. B 49 (1993) 787–794, http://dx.doi.org/10.1107/S0108768192006670.

[39] M. Nespolo, M.I. Aroyo, The crystallographic chameleon: when space groups change skin, Acta Crystallogr. A 72 (2016) 523–538, http://dx.doi.org/10.1107/S2053273316009293.

[40] H.-G. Unruh, J. Stromich, Properties of the secondary order parameter in Rb_2ZnCl_4, Solid State Commun. 39 (1981) 737–740, http://dx.doi.org/10.1016/0038-1098(81)90447-6.

[41] I.D. Brown, Recent developments in the methods and applications of the bond valence model, Chem. Rev. 109 (2009) 6858–6919.

[42] W.H. Baur, The geometry of polyhedral distortions. Predictive relationships for the phosphate group, Acta Crystallogr. B 30 (1974) 1195–1215, http://dx.doi.org/10.1107/S0567740874004560.

[43] N.E. Brese, M. O'Keeffe, Bond-valence parameters for solids, Acta Crystall. Sect. B 47 (1991) 192–197, http://dx.doi.org/10.1107/S0108768190011041.

[44] S. Adams, Relationship between bond valence and bond softness of alkali halides and chalcogenides, Acta Crystall. Sect. B 57 (2001) 278–287, http://dx.doi.org/10.1107/S0108768101003068.

[45] B.J. Campbell, H.T. Stokes, D.E. Tanner, D.M. Hatch, ISODISPLACE: a web-based tool for exploring structural distortions, J. Appl. Crystallogr. 39 (2006) 607–614, http://dx.doi.org/10.1107/S0021889806014075.

[46] H.T. Stokes, D.M. Hatch, B.J. Campbell, Isodistort, ISOTROPY software suite, 2024, URL.